JOURNAL OF SPACECRAFT AND ROCKETS
Vol. 31, No. 5, September–October 1994

# Hypersonic Convective Heat Transfer over 140-deg Blunt Cones in Different Gases

D. A. Stewart*
*NASA Ames Research Center, Moffett Field, California 94035*
and
Y. K. Chen*
*Eloret Institute, Palo Alto, California 94303*

**Large-angle blunt cones, with various corner radii, were tested in dissociated air, $CO_2$, and $CO_2$-Ar gas mixtures. These experiments were conducted at angles of attack from 0 to 20 deg. Heating distribution data and bow shock-wave geometry were obtained during exposure of the cones to the three gases. The data can be used to partially validate two-dimensional (2-D) axisymmetric and three-dimensional Navier-Stokes solutions of the heating distribution over a 140-deg blunt cone in a simulated Martian atmosphere. The predicted heating distribution over the cones and estimated bow shock standoff distances using a 2-D axisymmetric Navier-Stokes code were compared with test data taken at zero angle of attack.**

## Nomenclature

| | |
|---|---|
| $A$ | = area, $cm^2$ |
| $C_p$ | = specific heat, $J/kg \cdot K$ |
| $d$ | = diameter, cm |
| $H$ | = enthalpy, MJ/kg |
| $M$ | = Mach number |
| $P$ | = pressure, atm |
| $q$ | = heat-transfer rate, $W/cm^2 \cdot s$ |
| $R$ | = radius, cm |
| $S$ | = arc length, cm |
| $T$ | = temperature, K |
| $t$ | = time, s |
| $U$ | = velocity, cm/s |
| $\alpha$ | = angle of attack, deg |
| $\Delta$ | = standoff distance, cm |
| $\rho$ | = density, $g/cm^3$ |
| $\tau$ | = wall thickness, cm |

*Subscripts*

| | |
|---|---|
| b | = base |
| c | = corner |
| hem | = hemisphere |
| n | = nose |
| t | = total |
| sc | = sphere-cone |
| w | = wall |
| $\infty$ | = freestream condition |
| * | = sonic point |
| 0 | = stagnation point |

## Introduction

THE Mars Environmental Survey Vehicle (MESUR) is being proposed for a Martian entry near the end of this century.[1–3] The proposed configuration for MESUR is a large-angle blunt cone (140-deg included angle) with a base radius of approximately 2.0 m and a nose bluntness ratio of $R_n/R_b = 0.5$. The convective heat flux to the MESUR forebody heat shield during its high-speed aerobraking maneuvers into the Mars atmosphere results from both sensible and chemical heating. Sensible heating to the stagnation point of a large-angle blunt cone has been shown to be dependent on the cone angle and the bluntness ratio $R_c/R_b$.[4–7] Chemical heating is dependent upon the surface catalytic efficiency of the material chosen for the thermal protection system (TPS). Experimental heating data for use in the determination of a final MESUR configuration are lacking. To partially fill this need, heating distribution data obtained from blunt cones with various corner radii are presented in this paper. These data were obtained from tests conducted in the Ames 42-Inch Shock Tunnel using air, $CO_2$, and $CO_2$-Ar gas mixtures. Some of the data are compared with predicted heating distributions calculated using a Navier-Stokes solution.[8,9]

## Experimental and Computational Methods

### Facility Description

The Ames 42-inch shock-tunnel used combustion-heated gas (stoichiometric mixture of hydrogen, oxygen, and helium) to produce a reflected-shock, tailored-interface reservoir of test gas at the end of a shock tube 12.2 m long and 15.75 cm in diameter.[10–15] The test gas was expanded from the reservoir through a conical nozzle (20-deg included angle) to generate hypersonic flow in the test section of the tunnel (Fig. 1). The area ratio ($A/A^*$) of nozzle exit to throat for this facility ranged from 5000 to 157,000. During each test, a 2.54-cm-diam copper hemisphere was exposed simultaneously with the test model in order to determine the repeatability of the test condition and duration of uncontaminated flow. The duration of uncontaminated flow in the test section was determined using a parameter $q$(bar) defined as

$$q(\text{bar}) = q_{\text{hem}}/H_t\sqrt{P_t} \tag{1}$$

A typical $q$(bar) history during a shock-tunnel test is plotted in Fig. 2. In this example, onset of contamination of the test gas by the driver gas is indicated by a decrease in $q$(bar) at roughly 16 ms. In general, the duration of uncontaminated flow in the facility varied between 10 and 20 ms. The exposure of the test models to the hypersonic flow was controlled using a squib-operated closure valve. The valve was made as an integral part of the nozzle and controlled the test time to within 2–3 ms.[1]

### Model Description

Photographs and sketches of the test models are shown in Figs. 3 and 4. The models consisted of an inner and outer section of thin-wall copper held together by two interlocking cylinders (0.158 cm thick). The cones had a nose radius of 3.81 cm, base radii ranging

Presented as Paper 93-2787 at the AIAA 28th Thermophysics Conference, Orlando, FL, July 6–9, 1993; received Aug. 24, 1993; revision received Jan. 13, 1994; accepted for publication Feb. 7, 1994. 

*Research Scientist.

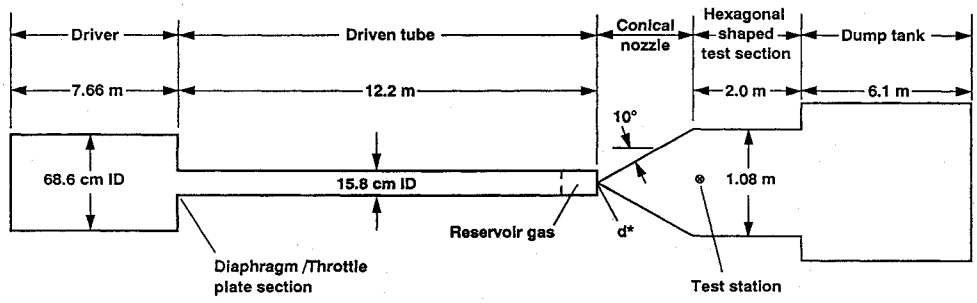


Fig. 1 Sketch of Ames 42-inch shock tunnel.

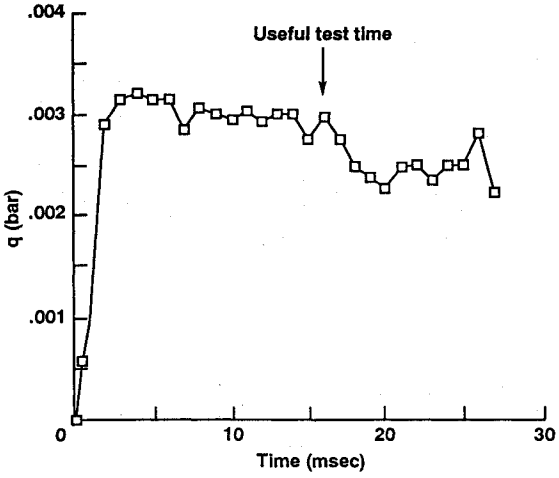


Fig. 2 Typical $q$(bar) history during shock-tunnel test in air.

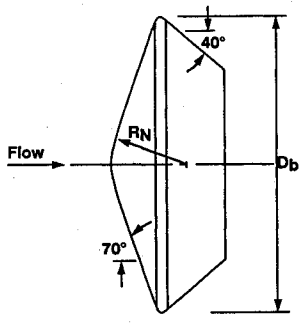


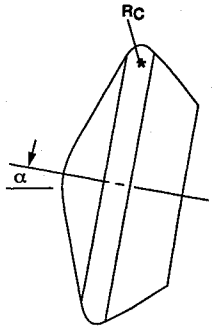


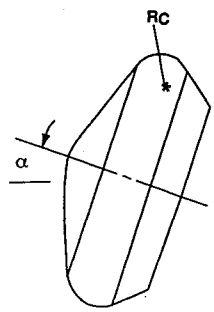


Fig. 3 Test configurations: a) $R_b/R_c = 0.0143$, b) $R_c/R_b = 0.0594$, and c) $R_c/R_b = 0.157$.

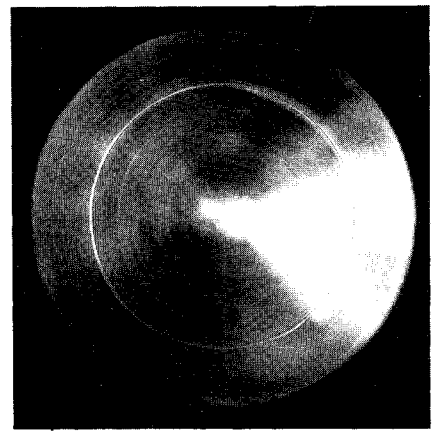


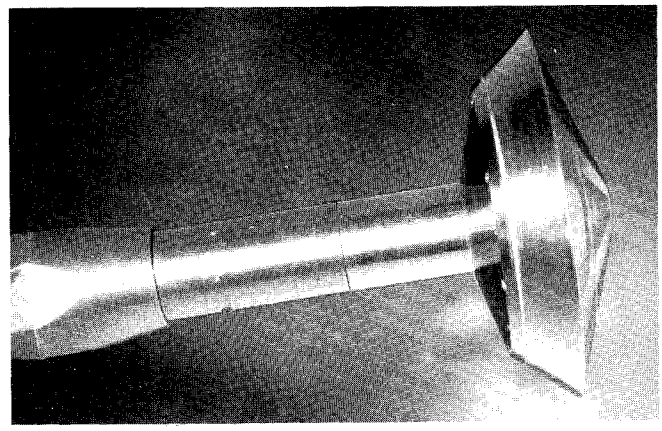


Fig. 4 Test model, $R_c/R_b = 0.0143$: a) front view and b) side view.

from 6.95 to 7.6 cm, and corner-to-base radius ratios of 0.0143 (Fig. 3a), 0.05943 (Fig. 3b), and 0.1572 (Fig. 3c). The corner radius was varied by changing the outer section of the model (Fig. 4). The thin-wall copper sections of the test models were made using an extruding process. The variation in wall thickness was maintained at less than 0.002 cm. The nominal wall thickness for the models was 0.043 cm. The models were mounted on an adjustable sting support, which was used to set angles of attack of 0, 10, or 20 deg (Fig. 4b).

The interlocking cylinder design resulted in models that had no structural component located near their corners. This design reduced conduction losses associated with the thermocouple measurements near the corners of the models. Twenty-five thermocouples were located in a single array along the axis of symmetry of the model. They extended in both directions from the geometric stagnation point to locations beyond the corner of the model (about midway along the 40-deg conical portion of the after body). Each thermocouple junction was formed by drilling two small holes (0.05 cm apart) in the model wall and then soldering a chromel wire in one and a constantan wire in the other hole, flush with the surface. This thermocouple installation, using no. 40 gauge wire, resulted in a time response of less than 1 ms to the heat flux at the model wall and the establishment

**Table 1 Freestream properties in 42-in. shock tunnel**

| Test gas | $M_\infty$ | $M_f$ | $d^*$, cm | $T_\infty$, K | $A/A^*$ | $P_0$, atm | $H_0$, MJ/kg | $q_{hem}$, W/cm$^2$ | $\rho_\infty$, kg/m$^3$ | $P_\infty$, atm | $U_\infty$, km/s | $Re_\infty$, $m^{-1}$ |
|---|---|---|---|---|---|---|---|---|---|---|---|---|
| Air | 14.9 | 3.8 | 1.02 | 190 | 10,500 | 0.05 | 9.3 | 220 | 3.1e−4 | 1.8e−4 | 4.15 | 9.9e+4 |
| $CO_2$ | 15.2 | 3.5 | 1.02 | 200 | 12,500 | 0.018 | 14.3 | 214 | 3.3e−4 | 1.6e−4 | 4.15 | 1.4e+5 |
| $CO_2$-Ar | 16.5 | 5.0 | 1.02 | 216 | 10,000 | 0.055 | 14.98 | 258 | 3.3e−4 | 1.4e−4 | 4.73 | 1.2e+5 |

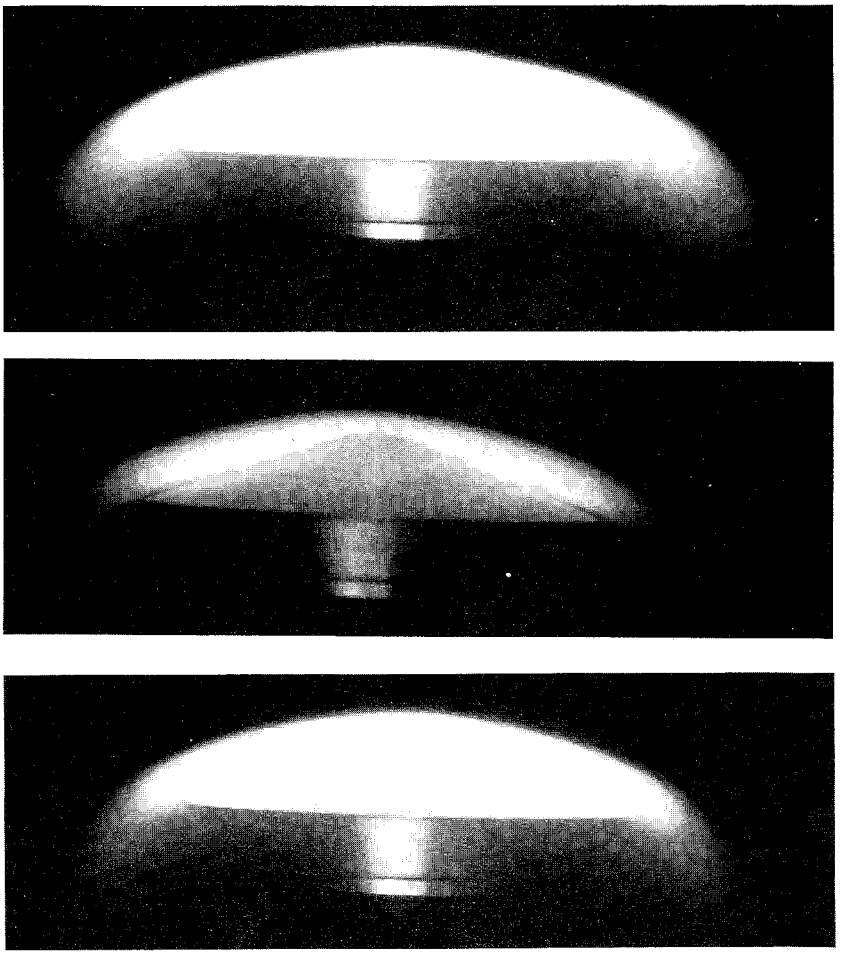


**Fig. 5 Photographs of test configuration (a) during shock-tunnel exposure, $\alpha = 0$: a) air, b) $CO_2$, and c) 73% $CO_2$-27% Ar.**

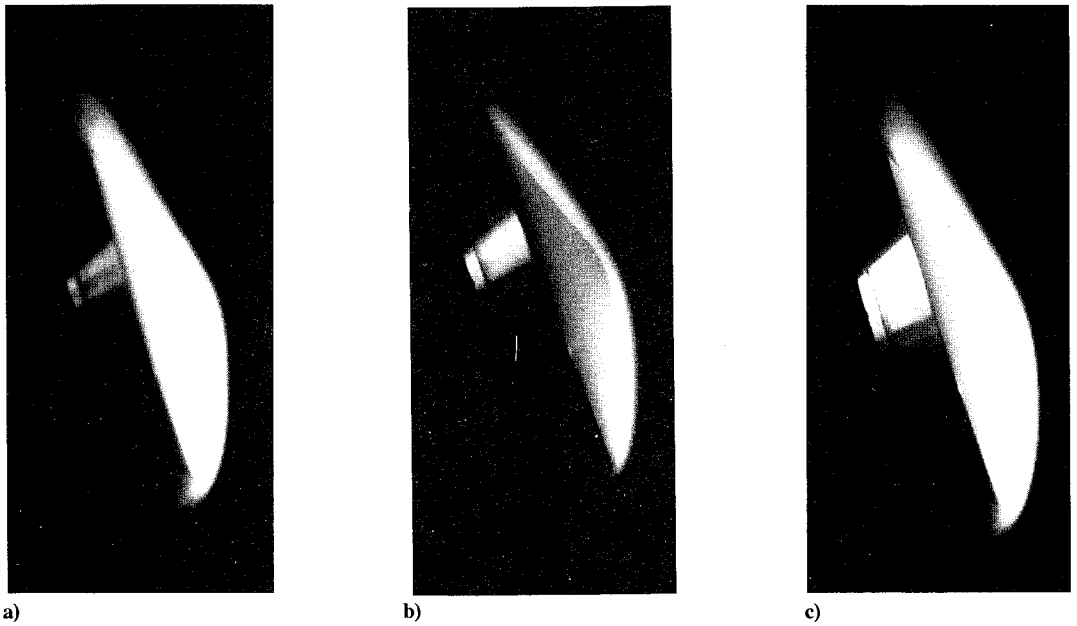


**Fig. 6 Photographs of test configuration (a) during shock-tunnel exposure, $\alpha = 20$ deg: a) air, b) $CO_2$, and c) 73% $CO_2$-27% Ar.**

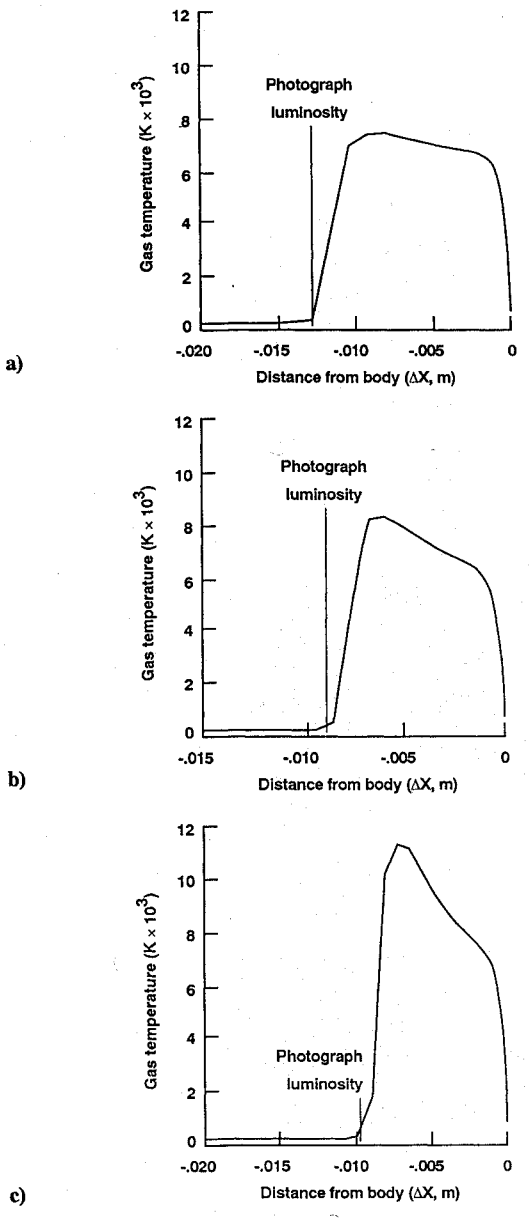


Fig. 7 Temperature profile along stagnation streamline: a) air, b) $CO_2$, and c) 73% $CO_2$–27% Ar.

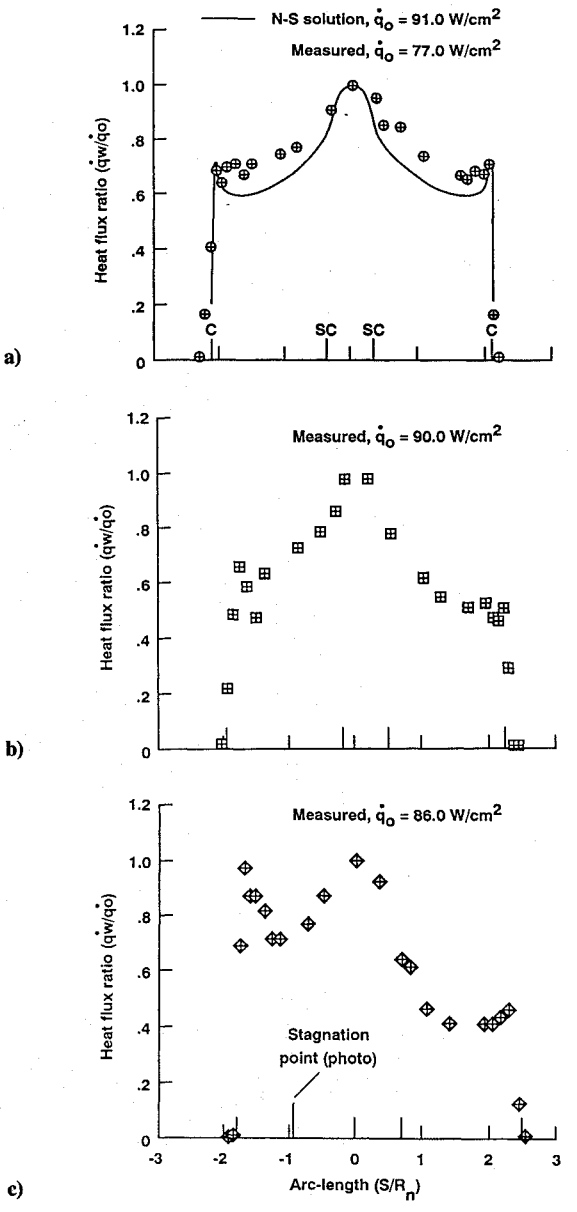


Fig. 8 Heating distribution over configuration (a) in air: a) $\alpha = 0$, b) $\alpha = 10$ deg, and c) $\alpha = 20$ deg.

of a linear slope on the measured temperature-time history within less than 4 ms after the start of flow into the test section.

## Experiment

The cones were tested in air, $CO_2$, and a 73% $CO_2$–27% Ar gas mixture at $\alpha = 0$, 10, and 20 deg. The reservoir pressure was approximately 290 atm for the three test gases, and the stagnation-point enthalpy ranged from 9.3 MJ/kg (air) to 14.96 MJ/kg ($CO_2$-Ar mixture). Reservoir and freestream properties were determined from an extensive tunnel calibration conducted for each gas or gas mixture.[13–15]

Thermocouple outputs from the model are amplified and recorded on a high-speed recorder during the 30-ms test exposure. The cold-wall heating distributions over the models were then determined using a seventh-order polynomial curve fit to the data and

$$q_w = \rho C_p \tau \frac{dT_w}{dt} \tag{2}$$

The temperature-time histories were obtained with the thermocouple arrays on the models positioned at roll angles of 0 and 180 deg. Average values from four separate tests were used to represent the reported heating distribution over the models. The maximum spread in $q_w$ for the four tests was ±10%.

## Analysis

Freestream conditions in front of the bow shock wave for the nonequilibrium flow were determined from one-dimensional computations of the gas expansion through the conical nozzle.[15] A frozen Mach number was used to define the gas properties. This concept is based on the assumption that most properties of the gas, having undergone relaxation of several internal degrees of freedom, are approximately the same as if the gas had made an instantaneous transition from full equilibrium flow to flow in which all internal energy exchange is frozen. In one-dimensional flow, this process can be characterized by a parameter called the frozen Mach number. This Mach number specifies the equilibrium speed of sound and constant entropy at which the expanding gas has made its transition to an internally frozen flow. In these tests, the freestream conditions were determined from a nozzle program[15] and measurements of impact pressure (hemisphere), static pressure (ogive cylinder), and freestream velocity.[13] The flow properties for these tests are summarized in Table 1.

Heating-rate distributions over the blunt cones at $\alpha = 0$, determined from the shock-tunnel tests, were compared with Navier-

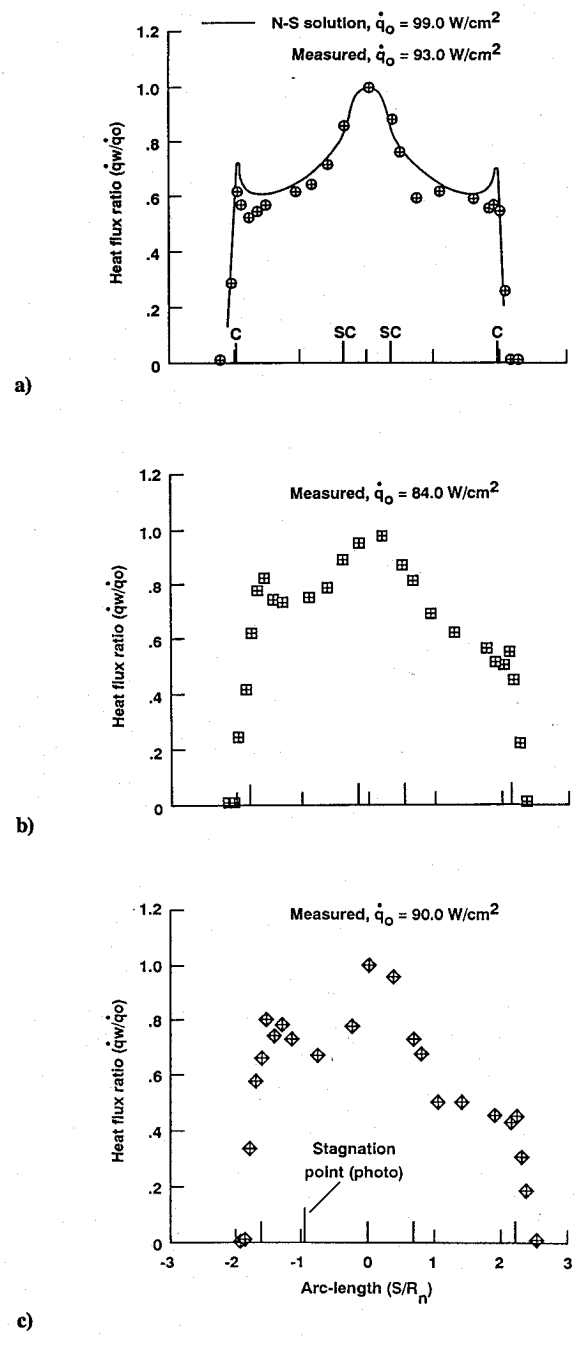


**Fig. 9 Heating distribution over configuration (b) in air: a) $\alpha = 0$, b) $\alpha = 10$ deg, and c) $\alpha = 20$ deg.**

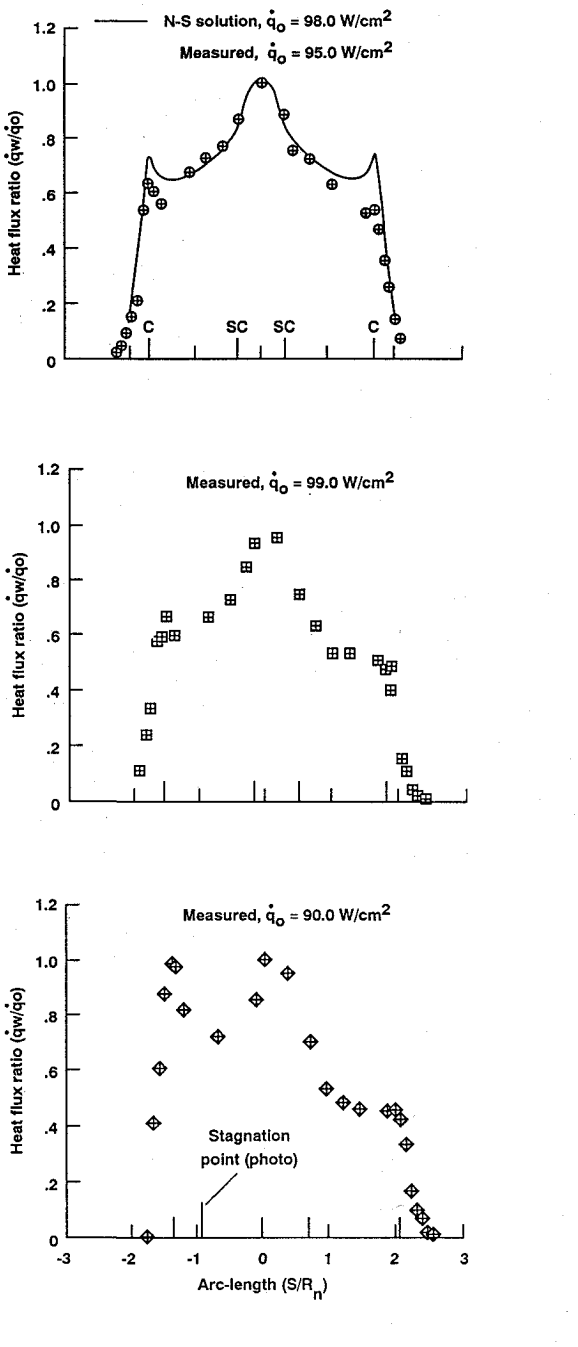


**Fig. 10 Heating distribution over configuration (c) in air: a) $\alpha = 0$, b) $\alpha = 10$ deg, and c) $\alpha = 20$ deg.**

Stokes (NS) solutions using the NSCAND computer code.[8] The governing equations used in the NSCAND code are essentially the two-dimensional axisymmetric NS equations expanded to allow for the presence of multiple species and two temperatures. The equations are solved in a fully implicit, flux-split, Gauss-Seidel line relaxation numerical technique. Five-species reacting air ($N_2$, $O_2$, NO, N, O) and $CO_2$ ($O_2$, O, CO, $CO_2$, C) models were used in the NS solutions. Ionization was not included in the NS solutions for the $CO_2$-Ar gas mixture, because it has been shown in a previous study to have a minimal effect on surface heating at these enthalpies.[8] Further work is needed to fully define the thermal and chemical gas properties in the nonequilibrium flowfield behind the bow shock wave generated by the $CO_2$ and $CO_2$-Ar gases. Therefore, the cold-wall heating rates to the surface of the copper models were calculated assuming radiation equilibrium and using oxygen and nitrogen atom recombination coefficients from the literature for the copper models (side-arm reactor data).[16,17] The atom recombination coefficient for CO + O was assumed equal to 1.0. A detailed description of the computational methods for the NS solutions are given in Refs. 8 and 9.

## Results and Discussion

### Shock Shapes

The stagnation-point heat-transfer rate to a high-angle blunt cone is affected by the position of the bow shock wave and the test environment. High-speed photographs of the 140-deg blunt cone, with $R_c/R_b = 0.0143$, were taken at $\alpha = 0$ and 20 deg in air, $CO_2$, and the $CO_2$-Ar gas mixture (see Figs. 5 and 6). Since the photographs were taken in less than a millisecond, it is assumed that the illuminance of the gases in front of the model indicates the shape and position of the bow shock wave at that particular instant. Figure 5 shows that at $\alpha = 0$ deg the bow shock wave is spherical in shape and symmetrical over the forebody of the cone. The standoff distance is greater for air ($\Delta/R_b = 0.13$) than for $CO_2$ ($\Delta/R_b = 0.09$). Photographs

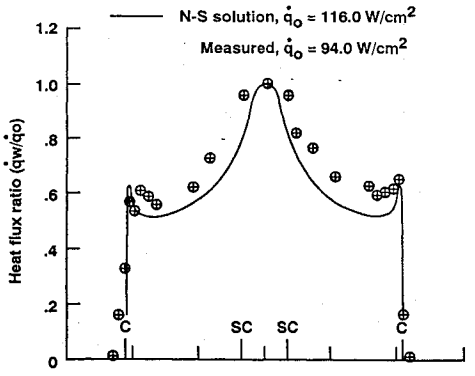


a)

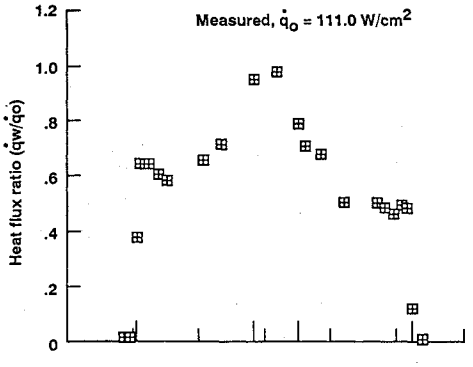


b)

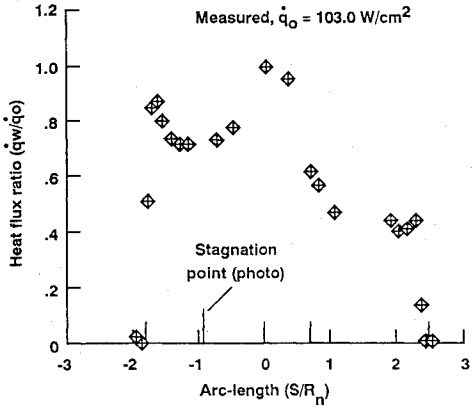


c)

**Fig. 11 Heating distribution over configuration (a) in $CO_2$: a) $\alpha = 0$, b) $\alpha = 10$ deg, and c) $\alpha = 20$ deg.**

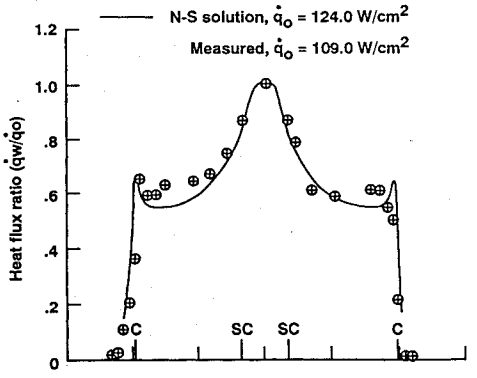


a)

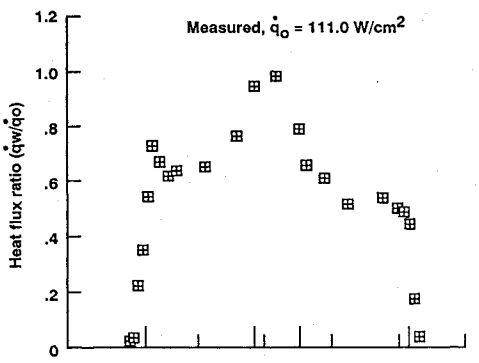


b)

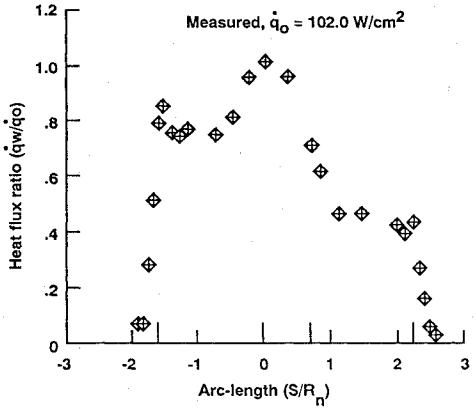


c)

**Fig. 12 Heating distribution over configuration (b) in $CO_2$: a) $\alpha = 0$, b) $\alpha = 10$ deg, and c) $\alpha = 20$ deg.**

taken with the model at $\alpha = 20$ deg show the three-dimensionality of the flow field in front the model during exposure to all three test gases (Fig. 6). Increase in angle of attack resulted in an increase in the bow shock-wave standoff distance from $\Delta/R_b = 0.13$ to $\Delta/R_b = 0.19$ for air and from $\Delta/R_b = 0.09$ to $\Delta/R_b = 0.13$ for $CO_2$. Note that at this angle of attack the windward side of the cone is perpendicular to the flow direction of the hypersonic stream. The shape of the bow shock wave is spherical over the windward surface and conical over the leeward surface of the forebody. Maximum slope of the bow wave relative to the freestream occurs at approximately the midpoint between the nose and corner of the cone on the windward surface. This suggests that the stagnation point on the model has moved from the model's axis of symmetry (centerline) at $\alpha = 0$ to a point approximately midway along the conical section of the forebody at $\alpha = 20$ deg. Computations by Weilmuenster and Hamilton also predicted a similar location for the stagnation point on a 140-deg blunt cone tested at $\alpha = 20$ deg in air.[18]

Bow shock-wave standoff distances, measured from the photographs taken with the models at $\alpha = 0$, are compared with values obtained from calculated temperature profiles along the stagnation streamline over the front surface of the models (Fig. 7). Predicted standoff distances from the NSCAND code agree well with those obtained from the photographs. Predicted heat-transfer rate distributions over these cones at $\alpha = 0$ were also compared with values obtained from the shock-tunnel tests.

### Stagnation-Point Heating

The calculated heating-rate distributions over each model, determined using shock-tunnel data, are plotted in Figs. 8 through 10 (air), 11 through 13 ($CO_2$), and 14 through 16 (73% $CO_2$–27% Ar). These calculated values are referred to as test data. In each figure the data represent the measured heating distribution for a cone with a particular corner radius that has been exposed to a selected gas at the

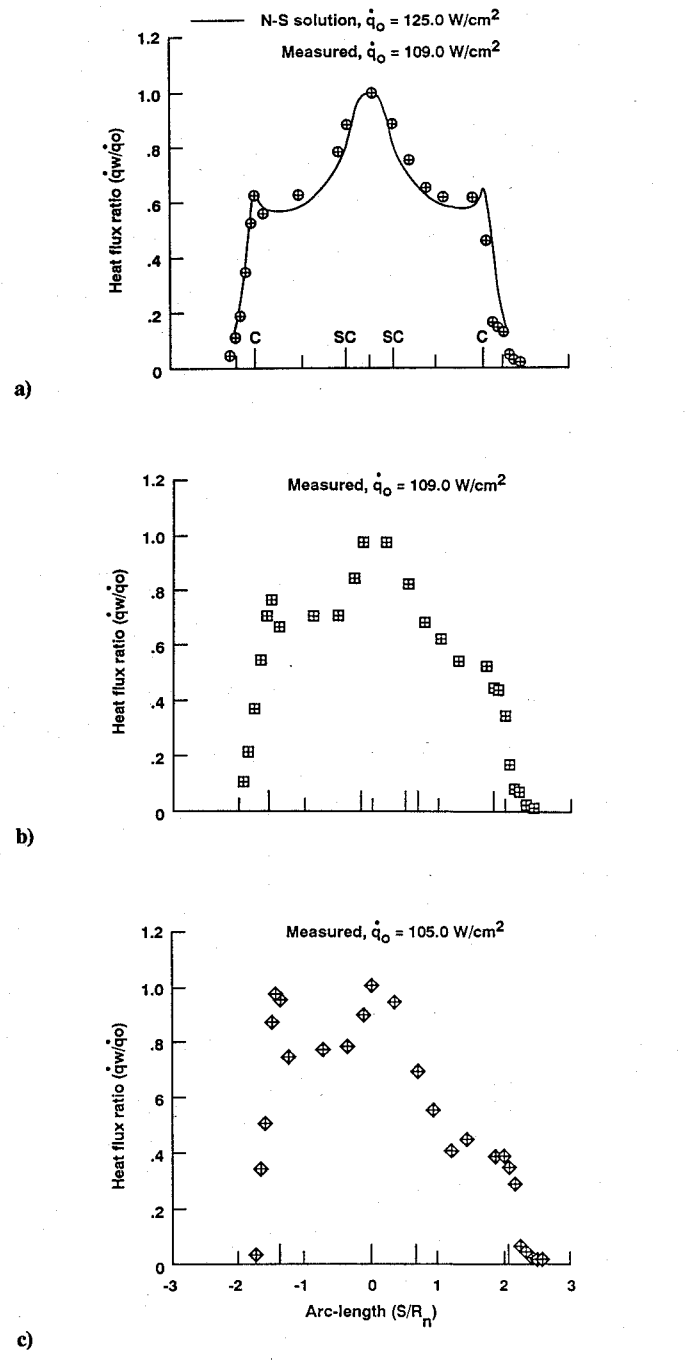


Fig. 13 Heating distribution over configuration (c) in $CO_2$: a) $\alpha = 0$, b) $\alpha = 10$ deg, and c) $\alpha = 20$ deg.

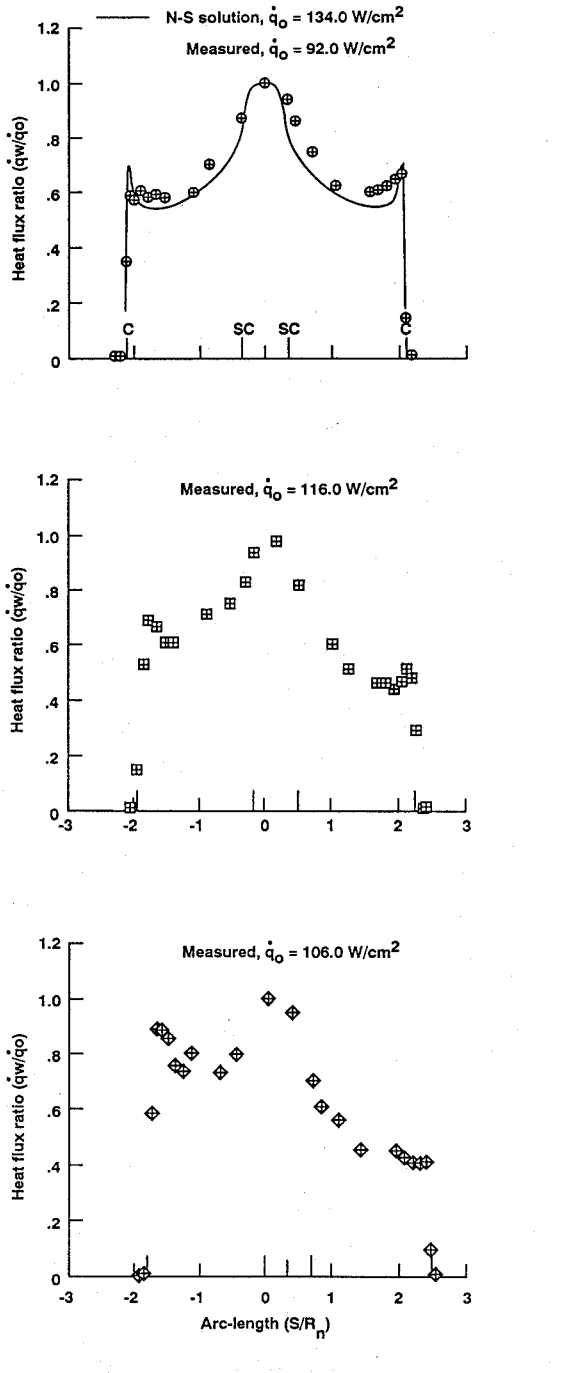


Fig. 14 Heating distribution over configuration (a) in 73% $CO_2$–27% Ar: a) $\alpha = 0$, b) $\alpha = 10$ deg, and c) $\alpha = 20$ deg.

three different angles of attack. These data were plotted relative to the arc-length ($S/R_n$), and they were normalized by the stagnation-point values obtained from the blunt cones ($q_w/q_0$). However, for models tested at $\alpha = 20$ deg, the data were normalized by a value corresponding to a point located at the sphere-cone junction and not the stagnation-point location. The origin of the arc length on the cones, tested at $\alpha = 20$ deg, was the sphere-cone junction. Negative and positive values of the arc length identify the windward and leeward sides of the cone's forebody, respectively.

The values used to normalize the data are given in Table 2. Included in the table are stagnation-point values calculated using NSCAND solutions for $\alpha = 0$. These values overpredict the data from the shock tunnel by as much as 25%. In general, data taken from configuration (a) in Fig. 2 and at $\alpha = 0$ were lower than the values obtained from the two cones with the larger corner radii. Stagnation-point heat-transfer rates to the cones with the two larger corner radii appear independent of the angle of attack; however, they are dependent on the test gas. The increased heating to the cones with the larger corner radii is the result of the change in position of the sonic point to a location closer to the stagnation point. The stagnation-point heat-transfer rate increased as a result of the corresponding increase in the velocity gradient and decrease in bow shock-wave standoff distance. A similar effect of corner radius on the stagnation-point heat-transfer rate to flat-faced cylinders was observed in earlier studies.[6,7] However, it was less than the effect on the 140-deg blunt cones used in the present tests. The difference in base radius (<5%) between the cone configurations does not account for the difference in stagnation-point heat-transfer rate to the cones. The differences between the predicted values and the shock-tunnel data were partly due to the constructed grid near the corner of the cone and partly due to uncertainties in input properties (freestream, transport, surface, and gas kinetics)

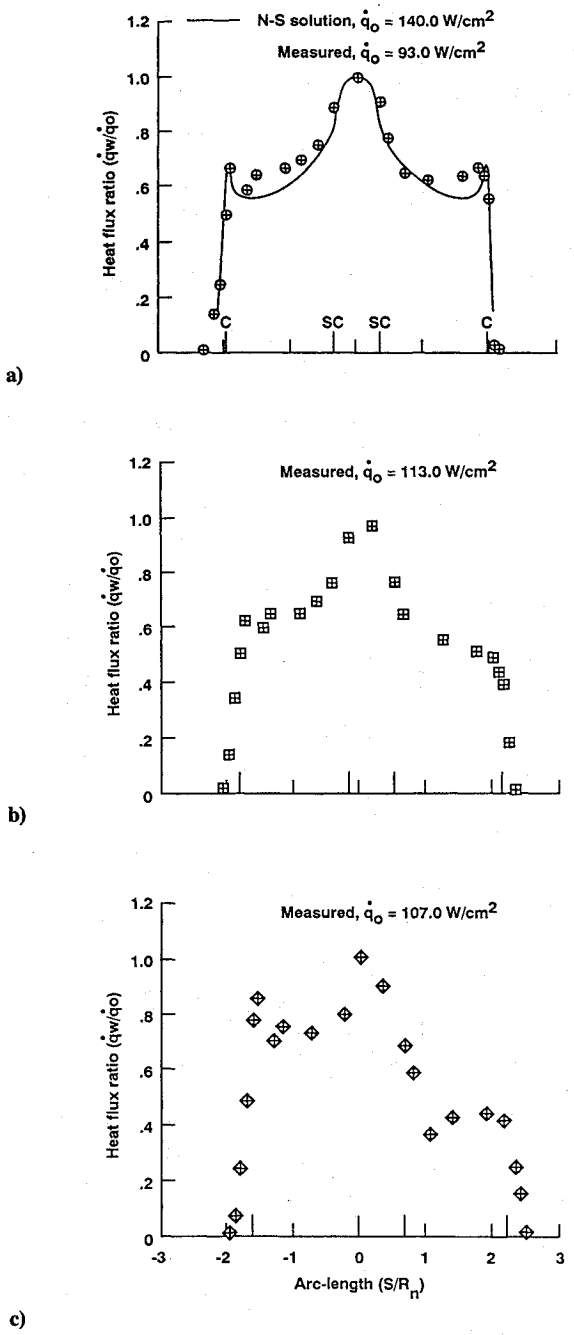


**Fig. 15 Heating distribution over configuration (b) in 73% $CO_2$–27% Ar: a) $\alpha = 0$, b) $\alpha = 10$ deg, and c) $\alpha = 20$ deg.**

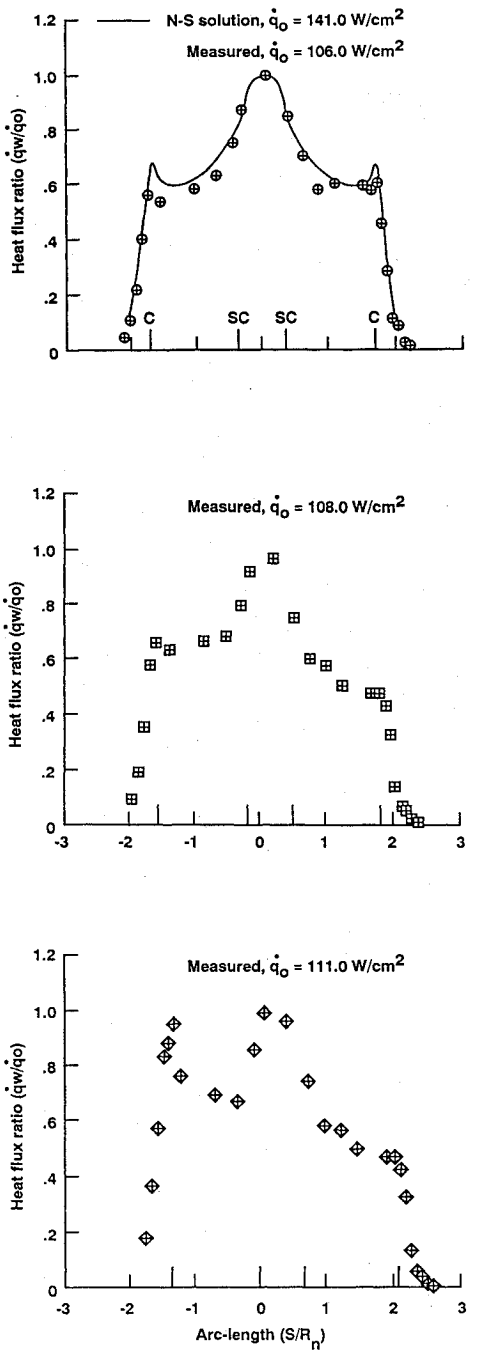


**Fig. 16 Heating distribution over configuration (c) in 73% $CO_2$–27% Ar: a) $\alpha = 0$, b) $\alpha = 10$ deg, and c) $\alpha = 20$ deg.**

used in the NS solution. However, the NS solutions clearly illustrate the effect of the corner radius on the stagnation-point heat-transfer rate.

## Heating-Rate Distribution

### Zero Angle of Attack

Predicted heating-rate distributions over the cones were compared with the test data. Predicted heating distributions for the two cones with the larger radii showed reasonably good agreement (<15%) with the test data taken from the three different gas environments. However, the NS solutions underpredicted the data taken from the cone with $R_c/R_b = 0.0143$ while being exposed to all three test gases (Figs. 8a, 11a, and 14a). The scatter in the data (low values) near the junction, between the inner and outer sections of the models, is attributed to conduction losses to the support structure ($1.141 > S/R_n < 1.230$) that was used to hold them together.

### Nonzero Angle of Attack

The heating distribution over the cones at $\alpha = 10$ and 20 deg could not be predicted using the present NS code. However, the following observations were made from the data. Heat-transfer rates to the forebody surface tended to increase toward the corner on the windward side and decrease on the leeward side of the model with increasing angle of attack. Higher heating rates at the windward corner of the model are attributed to the high local pressure gradients existing in this area of the model due to the rapid expansion of the gas. At $\alpha = 20$ deg (Fig. 6c) the conical section of the model is perpendicular to the flow direction and the stagnation point is located midway along the conical section of the cone. The heat-transfer rates (Fig. 8c) increase as the flow moves away from the stagnation point and approaches the Mach lines located on the spherical nose cap and the windward corner of the model. Again, the increased heat-

**Table 2 Stagnation-point heat-transfer rates to the blunt cones[a]**

| Test gas | $P_a/R_b$ | $q_0$, W/cm$^2$ (measured) $\alpha = 0$ | 10 deg | 20 deg | $q_0$, W/cm$^2$ (calculated) $\alpha = 0$ |
|---|---|---|---|---|---|
| Air | 0.0143 | 77 | 90 | 86[b] | $\tilde{9}1$ |
| Air | 0.0594 | 93 | 84 | 90[b] | $\tilde{9}9$ |
| Air | 0.1572 | 95 | 99 | 90[b] | $\tilde{9}8$ |
| $CO_2$ | 0.0143 | 94 | 111 | 103[b] | 116 |
| $CO_2$ | 0.0594 | 109 | 111 | 102[b] | 124 |
| $CO_2$ | 0.1572 | 109 | 109 | 105[b] | 125 |
| $CO_2$–Ar | 0.0143 | 92 | 116 | 106[b] | 134 |
| $CO_2$–Ar | 0.0594 | 83 | 113 | 107[b] | 140 |
| $CO_2$–Ar | 0.1572 | 106 | 108 | 111[b] | 141 |

[a]Data uncertainty ±10%.
[b]Heat-transfer rate at the sphere-cone junction (not stagnation-point value).

transfer rates over these regions of the model resulted from increased pressure gradients caused by the flow moving rapidly from subsonic to supersonic conditions. Also, Fig. 8c shows that on the leeward side of the model, the heat-transfer rates decrease over the conical section and again as the supersonic flow is further expanded around the corner. A similar trend in the heating distribution was observed over all the cones during their exposure to all three test gases at $\alpha = 20$ deg.

## Conclusions

In general the data showed that during the testing in all three test gases, the stagnation-point heat-transfer rate to the cones was directly affected by the corner radius. Also, the data showed that with the models at $\alpha = 20$ deg, the stagnation-point value (located near the midpoint of the conical section) was 30% lower than the value observed at the sphere-cone junction.

The measured stagnation-point heat transfer rates obtained from the models in air and at angle of attack $\alpha = 0$ agreed well with values predicted by the NSCAND code for cone configurations (b) and (c) in Fig. 4. However, the NSCAND code overpredicted the stagnation-point values obtained from the shock-tunnel data in all other test cases.

Data taken at $\alpha = 0$ showed reasonably good agreement with the predicted normalized heating-distribution profiles over cone configurations (b) and (c) in Fig. 4. However, the NSCAND solutions for the cone with the smallest corner radius underpredicted the normalized values obtained from the shock-tunnel data for all three test gases. At higher angles of attack, a full three-dimensional NS code is required in order to predict accurately the stagnation-point heat transfer rate as well as the heating distribution over a 140-deg blunt cone. In addition, better estimates of the atom recombination coefficients for the dissociated $CO_2$ and $CO_2$-Ar mixture are needed in order to better evaluate the effect of surface catalysis on the heat-transfer rates to these large-angle blunt cones.

## References

[1]Cooper, D. M., and Arnold, J. O., "Technologies for Aerobraking," 41st Congress of the International Astronautical Federation, Paper IAF-90-037, 1990.

[2]Walberg, G. D., "Aero-Capture for Manned Mars Missions—Status and Challenges," AIAA Paper 91-2870.

[3]Tauber, M., Henline, W., Chargin, M., Papadopoulos, P., Chen, Y. K., Yang, L., and Hamm, K., "MESUR Probe Aerobraking Preliminary Design Study," AIAA Paper 92-2952, 1992.

[4]Stewart, D. A., and Marvin, J. G., "Convective Heat-Transfer Rates on Large-Angle Conical Bodies at Hypersonic Speeds," NASA TN D-5526, 1969.

[5]Stewart, D. A., and Kolodziej, P., "Heating Distribution Comparison between Asymmetric and Symmetric Blunt Cones," AAIA Paper 86-1307, 1986.

[6]Zoby, E. V., and Sullian, E. M., "Effect of Corner Radius on Stagnation Point Velocity Gradients on Blunt Axisymmetric Bodies," NASA TM X-1067, 1966.

[7]Inouye, M., and Marvin, J. G., "Comparison of Experimental and Theoretical Shock Shapes and Pressure Distributions on Flat-Faced Cylinders at Mach 10.5," NASA TN D-4397, 1968.

[8]Candler, G. V., and MacCormack, R. W., "The Computation of Hypersonic Ionized Flows in Chemical and Thermal Nonequilibrium," AIAA Paper 88-0511, 1988.

[9]Chen, Y. K., Henline, W. D., Stewart, D. A., and Candler, G. V., "Navier-Stokes Solutions with Surface Catalysis for Martian Atmospheric Entry," AIAA 92-2946, 1992.

[10]Loubsky, W. J., Hiers, R. S., and Stewart, D. A., "Performance of a Combustion Driven Shock Tunnel with Application to the Tailored-Interface Operating Conditions," *Proceedings of the Third Conference on Performance of High Temperature Systems,* Dec. 7–9, 1964.

[11]Stewart, D. A., and Dannenberg, R. E., "A Note on Wire Ignition in Combustion-Heated Drivers for Shock-Tunnel Application," NASA TN D-3063, Oct. 1965.

[12]Dannenberg, R. E., and Stewart, D. A., "Techniques for Improving the Opening of the Main Diaphragm in a Large Combustion Driver," NASA TN D-2735, 1965.

[13]Hiers, R. S., Jr., and Reller, J. O., Jr., "Analysis of Non-equilibrium Air Streams in the Ames 1-Foot Shock Tunnel," NASA TN D-4985, 1969.

[14]Kussoy, M. I., Stewart, D. A., and Horstman, C. C., "Hypersonic Rarefied Flow over Sharp Slender Cones," NASA TN D-6689, 1972.

[15]Yoshikawa, K. K., and Katzen, E. D., "Charts for Air-Flow Properties in Equilibrium and Frozen Flows in Hypervelocity Nozzles," NASA TN D-693, 1961.

[16]Amman, H. H., Ph.D. Dissertation, Purdue Univ., 1964.

[17]Dickens, P. G., and Sutcliffe, M. B., *Transactions of the Faraday Society,* Vol. 60, pp. 1272–1285, 1964.

[18]Weilmuenster, K. J., and Hamilton, H. H., II, "A Comparison of Computed and Experimental Surface Pressure and Heating on 70° Sphere Cones at Angles of Attack to 20°," AIAA Paper 86-0567, Jan. 1986.